

Screening of knee-joint vibroarthrographic signals using statistical parameters and radial basis functions

Rangaraj M. Rangayyan · Y. F. Wu

Received: 10 April 2007 / Accepted: 4 October 2007 / Published online: 25 October 2007
© International Federation for Medical and Biological Engineering 2007

Abstract Externally detected vibroarthrographic (VAG) signals bear diagnostic information related to the roughness, softening, breakdown, or the state of lubrication of the articular cartilage surfaces of the knee joint. Analysis of VAG signals could provide quantitative indices for non-invasive diagnosis of articular cartilage breakdown and staging of osteoarthritis. We propose the use of statistical parameters of VAG signals, including the form factor involving the variance of the signal and its derivatives, skewness, kurtosis, and entropy, to classify VAG signals as normal or abnormal. With a database of 89 VAG signals, screening efficiency of up to 0.82 was achieved, in terms of the area under the receiver operating characteristics curve, using a neural network classifier based on radial basis functions.

Keywords Entropy · Form factor · Knee-joint sounds · Kurtosis · Radial basis functions · Skewness · Vibroarthrography

1 Introduction

1.1 Diagnosis of knee-joint pathology

The knee joint is the most commonly injured or diseased joint in the human body [41]. Arthritic degeneration of injured knees is known to result from a variety of traumatic causes. Damage to the stabilizing ligaments of the knee, or to the shock-absorbing fibrocartilage pads (the menisci) are two common causes of deterioration of knee-joint surfaces [39, 50]. Nontraumatic conditions of the knee could also lead to osteoarthritis, in which the articular cartilage softens, fibrillates, and sheds off the surface of the patella, femur, or the tibia, contributing to painful inflammation of the joint. Defining treatment protocols for conditions as above is often difficult, because the natural history of their progression in an individual cannot be easily determined. Imaging techniques such as X-ray, computed tomography, and magnetic resonance imaging (MRI) can assist in the noninvasive detection of major cartilage pathology, but cannot be routinely used in clinical practice for screening patients or to characterize the functional integrity of cartilage, in terms of softening, stiffness, or fissuring. Arthrography (dye-enhanced X-ray visualization of articular cartilage surfaces and menisci) and enhanced MRI, both semi-invasive procedures, are more specific for the detection of cartilage defects, but suffer from limitations in terms of defining functional changes over time. Arthroscopy has emerged as the gold standard for relatively low-risk assessment of joint surfaces (meniscal and chondral) in order to determine the prognosis and treatment for a variety of conditions [25, 38]. Regardless, arthroscopy is not a practical procedure for repeated examination of patients over time, because it is invasive and does carry risks.

R. M. Rangayyan (✉)
Department of Electrical and Computer Engineering Schulich
School of Engineering, 2500 University Dr. NW University
of Calgary, Calgary, AB, Canada T2N 1N4
e-mail: ranga@ucalgary.ca

Y. F. Wu
School of Information Engineering, Beijing University of Posts
and Telecommunications, 10 Xi Tu Cheng Road,
Haidian District, Beijing 100876, China
e-mail: y.wu@ieee.org

1.2 Knee-joint vibration signals

Mechanical vibrations emitted from knee joints during flexion or extension are expected to be associated with pathological conditions in the knee joint, and may be useful indicators of the roughness, softening, breakdown, or the state of lubrication of the articular cartilage surfaces [8, 9, 17, 19, 49, 60, 61]. Externally detected vibration signals may provide a useful index of early joint degeneration or disease. With appropriately standardized signal recording and processing methods, computer-aided analysis of knee-joint vibration or vibroarthrographic (VAG) signals could provide quantitative indices for noninvasive diagnosis of articular cartilage breakdown, and thus, noninvasive staging of osteoarthritis in the knee. Detection and localization of knee-joint pathology via the analysis of VAG signals could decrease the need for diagnostic surgery, and could also be useful in monitoring joint function and cartilage deterioration over extended periods of time.

When a knee joint is flexed or extended, both the intra- and extra-articular components may produce vibration signals (or sounds) as they pass over one another [13, 18, 19, 24, 33, 48, 58]. The diagnostic potential of knee-joint sounds for noninvasive characterization of articular cartilage disorders was first reported by Blodgett [9] in 1902. The first measurement of knee-joint signals was reported by Erb in 1933 [17]. Since then, significant progress has been made in data acquisition and signal processing [11, 14, 19, 24, 41, 47, 56, 62], adaptive cancellation of muscle interference from the VAG signal [65], localization of sound source and pathology [59], auditory mapping and display of VAG signals [35], and parametric representation and screening of VAG signals [34, 36, 45, 54, 63].

There is renewed interest, among orthopedic surgeons and developers of aids for the musculo-skeletal system, in the use of VAG signals for noninvasive screening of patients presenting with complaints related to the knee joint, prior to the recommendation of arthroscopic examination. This arises from the clinical observation that a significant portion of the patients who undergo arthroscopy are seen to be free of any abnormality of the joint [38]. With the aim of developing a screening tool for use in the clinic of a physician or an orthopedic specialist, we investigate the use of several statistical parameters for normal-versus-abnormal classification of VAG signals. Improved selection of patients for arthroscopy should reduce the associated costs to the healthcare system and the concomitant risks to the patient. In order to simplify the signal processing and decision-making steps, as well as to minimize the clinical information required in the design or application of the methods, we propose to analyze VAG signals without performing adaptive segmentation or associating parts of the signals with specific parts of the articular cartilage surfaces

and related pathology. The proposed features are based on clinical and visual observations of the nature of normal and abnormal VAG signals [55].

2 Methods

2.1 VAG signal data acquisition

Each subject sat on a rigid table in a relaxed position with the leg being tested freely suspended in air. The VAG signal was recorded by placing an accelerometer (model 3115a, Dytran, Chatsworth, CA, USA) at the mid-patella position of the knee as the subject swung the leg over an approximate angle range of 135° (approximately full flexion) to 0° (full extension) and back to 135° in 4 s [37, 54]. The first half (approximately) of each VAG signal corresponds to extension, and the second half to flexion of the leg. Auscultation of the knee joint using a stethoscope was also performed, and a qualitative description of sound intensity and type was recorded, along with their relationship to joint angle. Informed consent was obtained from each subject. The experimental protocol was approved by the Conjoint Health Research Ethics Board of the University of Calgary.

The VAG signal was prefiltered (10 Hz to 1 kHz) and amplified before digitizing at a sampling rate of 2 kHz. Each signal was normalized to the amplitude range [0, 1]. Figure 1 shows examples of normal and abnormal VAG signals. The abnormal signal exhibits a higher degree of overall variability and complexity than the normal signal.

The database used in the present study consists of 89 signals, with 51 from normal volunteers and 38 from subjects with knee-joint pathology. The normals were established by clinical examination and history. The abnormal signals were collected from symptomatic patients scheduled to undergo arthroscopy independent of the VAG studies. The abnormal signals include chondromalacia of different grades at the patella, meniscal tear, tibial chondromalacia, and anterior cruciate ligament injuries, as confirmed during arthroscopic examination.

The power and other characteristics of VAG signals vary with the nature and severity of the associated pathology. The dataset available is not adequate to permit classification of the signals into various types or stages of pathology. The present study is aimed at screening only, that is, normal versus abnormal classification; therefore, no restriction is imposed on the type of pathology.

As compared to previous related studies [34, 36, 54], the dataset used in the present study lacks one abnormal VAG signal due to corruption of the data. The present study uses the same dataset as that used in a recent report by Umaphathy and Krishnan [63].

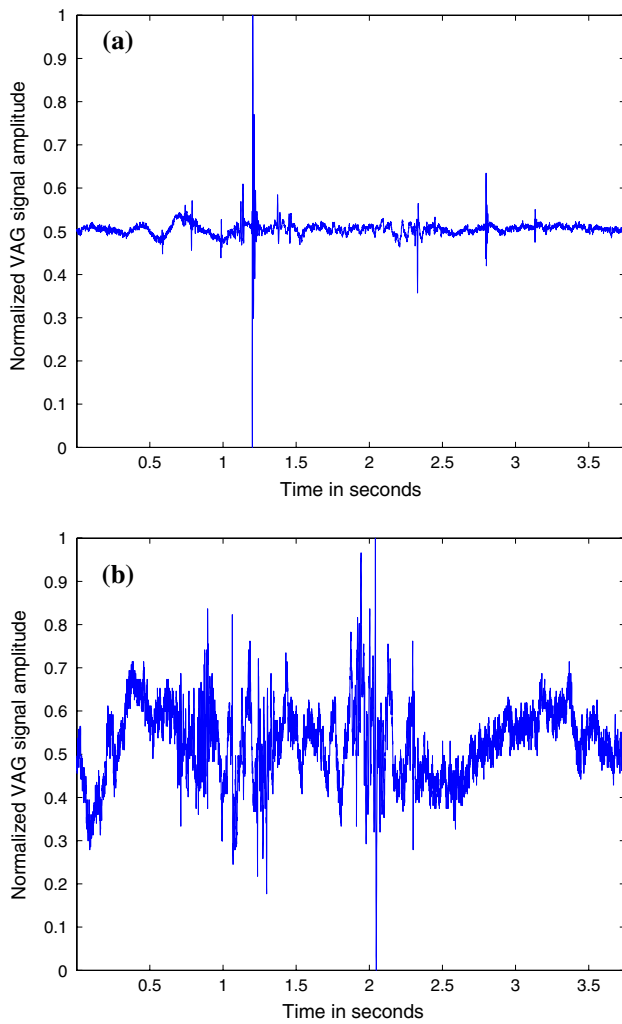


Fig. 1 VAG signal examples: **a** of a normal subject; **b** of a patient with knee-joint pathology. The amplitudes have been normalized to the range [0, 1]

2.2 Feature extraction from VAG signals

Figure 2 shows the normalized histograms of the VAG signals in Fig. 1. It is evident that the abnormal signal has a broader range of significant values than the normal signal.

In order to characterize the larger variability observed in abnormal VAG signals, as compared to normal signals, the standard deviation or variance of the signals could be used. An improved representation of the variability or “busyness” of a signal may be achieved via the measure of form factor (FF), which was originally defined by Hjorth [21–23]; see also Cooper et al. [15] and Rangayyan [51]. FF is defined using three parameters. The first parameter, *activity*, is the variance σ_x^2 of the given signal x (defined below). The second parameter, *mobility* M_x , is computed as the square root of the ratio of the activity of the first derivative x' of the signal to the activity of the original signal:

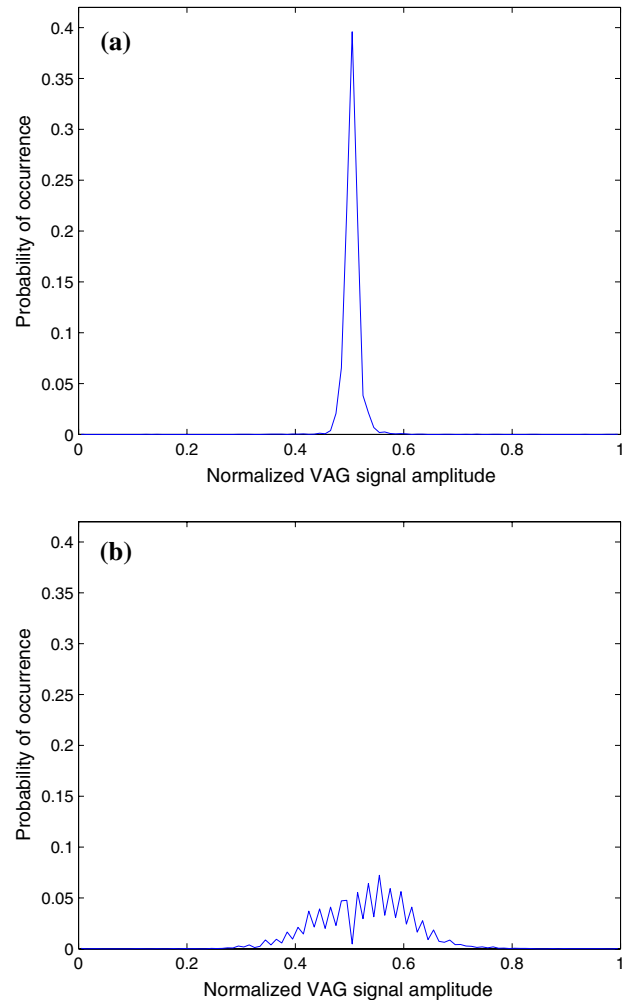


Fig. 2 Normalized histograms of the VAG signals in Fig. 1: **a** normal, **b** abnormal

$$M_x = \left[\frac{\sigma_{x'}^2}{\sigma_x^2} \right]^{\frac{1}{2}} = \frac{\sigma_{x'}}{\sigma_x}. \tag{1}$$

The third parameter, *complexity* or FF, is defined as the ratio of the mobility of the first derivative of the signal to the mobility of the signal itself:

$$FF = \frac{M_{x'}}{M_x} = \frac{\sigma_{x''}/\sigma_{x'}}{\sigma_{x'}/\sigma_x}, \tag{2}$$

where x'' is the second derivative of x .

The FF value of a pure sinusoid is unity; other signals have FF values that increase with the extent of their variability or complexity. However, because the computation of FF is based upon the first and second derivatives of the given signal and their variances, the measure could be sensitive to noise.

Hjorth [21–23] described the mathematical relationships between the activity, mobility, complexity, and power

spectral density of a signal, and applied them to model the generation of electroencephalographic (EEG) signals. Binnie et al. [6, 7] proposed the application of FF to EEG analysis for the detection of epilepsy.

Vibroarthrographic signals generated during extension (approximately the first half of the duration of each signal recorded according to the protocol described in Sect. 2.1 and illustrated in Fig. 1) have been observed to bear more discriminant information than those related to flexion, due to increased loading of the knee joint during the former phase of swinging movement of the leg than the latter [37]. To account for this expected characteristic and verify the clinical observation, values of FF were also computed separately for the first half (extension) and second half (flexion) of each signal, and labeled as FF1 and FF2, respectively.

In order to characterize the differences observed between the histograms of normal and abnormal VAG signals, we use skewness (S), kurtosis (K), and entropy (H) [40, 52]. The measures are based upon the moments of the probability density function (PDF) of the given signal, denoted by $p_x(x_l)$, with $x_l, l = 0, 1, 2, \dots, L - 1$, representing the L bins used to represent the range of the values of the signal x . In the present work, we have set $L = 100$. The PDF of each signal was estimated by normalizing its histogram; see Fig. 2 for examples. The k th central moment of the PDF $p_x(x_l)$ is defined as

$$m_k = \sum_{l=0}^{L-1} (x_l - \mu_x)^k p_x(x_l), \quad (3)$$

where μ_x is the mean value, given by

$$\mu_x = \sum_{l=0}^{L-1} x_l p_x(x_l). \quad (4)$$

The variance is given by

$$\sigma_x^2 = m_2 = \sum_{l=0}^{L-1} (x_l - \mu_x)^2 p_x(x_l). \quad (5)$$

The normalized third and fourth moments, known as the skewness (S) and kurtosis (K), respectively, are defined as

$$S = \frac{m_3}{(m_2)^{3/2}}, \quad (6)$$

and

$$K = \frac{m_4}{(m_2)^2}. \quad (7)$$

Skewness is related to asymmetry of the PDF. Kurtosis is related to the presence of a long tail in the PDF; it also represents the “peakedness” of the PDF.

Entropy is a commonly used measure to represent the nature and spread of a PDF, and is defined as

$$H = - \sum_{l=0}^{L-1} p_x(x_l) \log_2[p_x(x_l)]. \quad (8)$$

The entropy is at its maximum for a uniform PDF, and has lower values for PDFs with narrow ranges of significant probability values.

Table 1 lists the values of the mean and standard deviation of each feature described above for the normal and abnormal signals in the dataset used. The results of application of pattern classification methods to the features are presented in Sect. 3.

2.3 Pattern classification

Receiver operating characteristics (ROC) curves were generated for each feature using the software tool ROCKIT provided by the University of Chicago [42, 43]. The area (A_z) under the ROC curve was derived to serve as a summary measure of the overall classification performance of each experiment.

A pattern classification experiment was conducted using Fisher’s linear discriminant analysis (FLDA) [16] using the set of features {FF1, FF2, S , K , H }, which was selected by using a genetic algorithm as the best set of features from all of the six features derived [46], including the leave-one-out (LOO) procedure for cross validation [16]. The resulting discriminant values were used to derive an ROC curve and the associated A_z value using ROCKIT.

Classification experiments were also conducted with several neural networks with radial basis functions (RBF) [20], using the set of features {FF1, FF2, S , K , H } and the LOO procedure. An RBF network (RBFN) with a feed-forward hidden layer (see Fig. 3) applies a nonlinear transformation from the input space to a high-dimensional

Table 1 Mean and standard deviation (SD) of the proposed features for the normal (51) and abnormal (38) VAG signals

Feature	Mean \pm SD: Normal signals	Mean \pm SD: Abnormal signals
FF	3.53 \pm 1.93	5.29 \pm 3.67
FF1	3.18 \pm 1.33	4.93 \pm 2.75
FF2	3.50 \pm 1.63	5.16 \pm 3.48
S	0.80 \pm 2.60	−0.27 \pm 1.22
K	71.67 \pm 172.42	25.46 \pm 57.22
H	4.05 \pm 1.07	4.39 \pm 0.93

FF, FF1, FF2: Form factor for the full duration, the first half (extension), and the second half (flexion), respectively. S Skewness, K kurtosis, H entropy

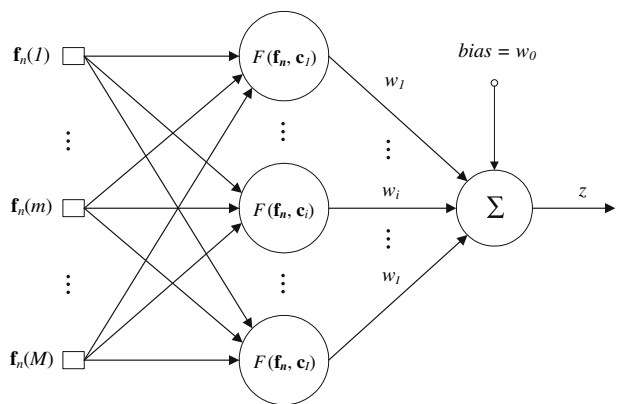


Fig. 3 Schematic representation of the RBF network used for the classification of VAG signals. The inputs to the RBFN, $f_n(1), f_n(2), \dots, f_n(M)$, are the M components of the feature vector \mathbf{f}_n of a VAG signal to be classified. The hidden layer has I neurons. Note: $F(\mathbf{f}_n, \mathbf{c}_i) = \phi(\mathbf{f}_n, \mathbf{c}_i)$ in the text

hidden space, and then produces separable responses through a linear output transformation.

Consider a set of N labeled input feature vectors, \mathbf{f}_n , $n = 1, 2, \dots, N$ (characterizing the $N = 89$ VAG signals in the present study), each of which is an $M \times 1$ vector. Let z_n be the desired classification response for the n th signal, represented by its feature vector \mathbf{f}_n . With reference to the RBFN shown in Fig. 3, we have the output of the network as

$$\hat{z}_n = \sum_{i=1}^I w_i \phi(\mathbf{f}_n, \mathbf{c}_i) + w_0, \tag{9}$$

where \hat{z}_n indicates an estimate of z_n , the RBF ϕ is defined as

$$\phi(\mathbf{f}_n, \mathbf{c}_i) = \exp\left(-\log_e(2) \frac{\|\mathbf{f}_n - \mathbf{c}_i\|^2}{\sigma^2}\right), \tag{10}$$

w_i is the weight and \mathbf{c}_i is the center vector for the i th neuron in the hidden layer, I is the number of neurons in the hidden layer, w_0 is the bias, and σ is the spread parameter that determines the width of the area in the input space to which each hidden neuron responds. For example, a neuron with a spread of 0.1 provides the output of 0.5 for any input vector \mathbf{f}_n at the distance of 0.1 from its weight vector.

The major challenge in the design of an RBFN is the selection of the centers. The selection of the centers in a random fashion commonly leads to a relatively large network with high computational complexity. In the present work, we applied the orthogonal least-squares (OLS) method [10], a systematic method for center selection which can significantly reduce the size of the RBFN.

According to Eq. 9, the mapping performed by the RBFN can be viewed as a regression model, expressed in matrix form as

$$\begin{bmatrix} z_1 \\ z_2 \\ \vdots \\ z_N \end{bmatrix} = \begin{bmatrix} 1 & \phi(\mathbf{f}_1, \mathbf{c}_1) & \cdots & \phi(\mathbf{f}_1, \mathbf{c}_I) \\ 1 & \phi(\mathbf{f}_2, \mathbf{c}_1) & \cdots & \phi(\mathbf{f}_2, \mathbf{c}_I) \\ \vdots & \vdots & \ddots & \vdots \\ 1 & \phi(\mathbf{f}_N, \mathbf{c}_1) & \cdots & \phi(\mathbf{f}_N, \mathbf{c}_I) \end{bmatrix} \begin{bmatrix} w_0 \\ w_1 \\ \vdots \\ w_I \end{bmatrix} + \begin{bmatrix} e_1 \\ e_2 \\ \vdots \\ e_N \end{bmatrix}, \tag{11}$$

which is equivalent to

$$\mathbf{z} = \Phi \mathbf{w} + \mathbf{e}, \tag{12}$$

where Φ is the $N \times (I + 1)$ regression matrix with the RBFs; \mathbf{z} represents the vectorial form of the corresponding values z_n for $n = 1, 2, \dots, N$; $\mathbf{w} = [w_0, w_1, \dots, w_I]^T$; and \mathbf{e} is the approximation error.

The centers of the RBFN are chosen from the set of input feature vectors (a total of $N = 89$ candidates). The task of the OLS method is to perform a systematic selection of less than N centers so that the network size can be reduced with minimal degradation of performance during the learning procedure. From Eq. 11, we can see that there is a one-to-one correspondence between the centers of the RBFN and the coefficients in the regression matrix Φ . At each step of the OLS regression, a new center can be selected in such a manner that the incremental variance of the desired output is maximized. Suppose that there are $Q < N$ centers selected. The OLS solution yielding the weights is given by [10]

$$\hat{\mathbf{w}} = (\Phi^T \Phi)^{-1} \Phi^T \mathbf{z} = \Phi^+ \mathbf{z}, \tag{13}$$

where Φ^+ represents the pseudoinverse of the regression matrix Φ . The output of the RBFN is then expressed as

$$\hat{\mathbf{z}} = \Phi \hat{\mathbf{w}} = [\Phi_1, \Phi_2, \dots, \Phi_Q] \hat{\mathbf{w}}, \tag{14}$$

where $\hat{\mathbf{z}}$ denotes the portion of \mathbf{z} that is within the vector space spanned by the columns ϕ_q of the regression matrix Φ .

By using Gram-Schmidt orthogonalization [20], the regression matrix can be decomposed as

$$\Phi = \mathbf{B} \mathbf{A} = [\mathbf{b}_1, \mathbf{b}_2, \dots, \mathbf{b}_Q] \begin{bmatrix} 1 & a_{11} & a_{12} & \cdots & a_{1Q} \\ 0 & 1 & a_{23} & \cdots & a_{2Q} \\ \vdots & \vdots & \ddots & \vdots & \vdots \\ 0 & 0 & 0 & \cdots & 1 \end{bmatrix}, \tag{15}$$

where \mathbf{A} is a $Q \times Q$ upper-triangular matrix with 1s on the main diagonal, and \mathbf{B} is an $N \times Q$ matrix with mutually orthogonal columns \mathbf{b}_q such that

$$\mathbf{B}^T \mathbf{B} = \mathbf{H} = \text{diag}[h_1, h_2, \dots, h_Q], \tag{16}$$

where the $Q \times Q$ matrix \mathbf{H} is a diagonal matrix with elements h_k given by

$$h_k = \mathbf{b}_k^T \mathbf{b}_k = \sum_{q=1}^N b_{kq}^2. \tag{17}$$

By substituting Eq. 15 into Eq. 12, we obtain

$$\mathbf{z} = \mathbf{B} \mathbf{A} \mathbf{w} + \mathbf{e} = \mathbf{B} \mathbf{g} + \mathbf{e}, \tag{18}$$

where $\mathbf{g} = \mathbf{A} \mathbf{w}$. In Eq. 18, the desired output vector \mathbf{z} is expressed as a linear combination of the mutually orthogonal columns of the matrix \mathbf{B} . The OLS solution for the coordinate vector \mathbf{g} is given by

$$\hat{\mathbf{g}} = (\mathbf{B}^T \mathbf{B})^{-1} \mathbf{B}^T \mathbf{z} = \mathbf{B}^+ \mathbf{z} = \mathbf{H}^{-1} \mathbf{B}^T \mathbf{z}. \tag{19}$$

The k th component of the vector $\hat{\mathbf{g}}$ is given by

$$g_k = \frac{\mathbf{b}_k^T \mathbf{z}}{\mathbf{b}_k^T \mathbf{b}_k}. \tag{20}$$

Because Gram–Schmidt orthogonalization ensures the orthogonality between the approximation error \mathbf{e} and $\mathbf{B} \mathbf{g}$ in Eq. 18, we have

$$\mathbf{z}^T \mathbf{z} = \mathbf{g}^T \mathbf{B}^T \mathbf{B} \mathbf{g} + \mathbf{e}^T \mathbf{e} = \mathbf{g}^T \mathbf{H} \mathbf{g} + \mathbf{e}^T \mathbf{e} = \sum_{k=1}^Q h_k g_k^2 + \mathbf{e}^T \mathbf{e}. \tag{21}$$

Because there is a one-to-one correspondence between the elements of the regression vector \mathbf{g} and the RBF centers \mathbf{c}_i , each term in the summation above reflects the contribution of each of the RBF centers. We can, therefore, define an error reduction ratio (err) with respect to the i th RBF center as [10]

$$\text{err}_i = \frac{h_i g_i^2}{\mathbf{z}^T \mathbf{z}}. \tag{22}$$

The error reduction ratio offers a simple and effective criterion for the selection of RBF centers in a regression model. At each step of the regression, an RBF center is selected so as to maximize the error reduction ratio toward a tolerance value.

The design details of the RBFN used in our experiments are as follows: The input layer contains $M = 5$ nodes to accept the set of features $\{\text{FF1}, \text{FF2}, S, K, H\}$ extracted from each VAG signal. The spread parameter σ was varied over the range [1, 6], and the number of hidden nodes I was varied over the range [1, 30]. The resulting output values were used to derive ROC curves and the associated A_z values using ROCKIT.

3 Results

Figure 4 shows the ROC plots for the individual features FF, FF1, FF2, and S . Table 2 lists the A_z values obtained for the various parameters tested. It is seen that FF1 and FF

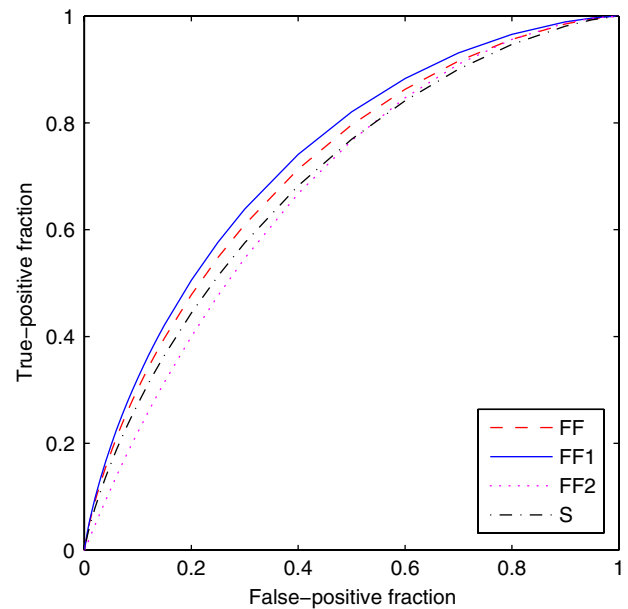


Fig. 4 ROC plots for the individual features FF, FF1, FF2, and S . The corresponding areas under the ROC curves (A_z) are 0.72, 0.73, 0.68, and 0.70, respectively

provide similar levels of classification performance with A_z values of 0.73 and 0.72, respectively, which are better than those provided by the remaining features individually. The higher accuracy provided by FF1 (0.73) than FF2 (0.68) confirms the expectation that the VAG signal contains more discriminant information during extension than flexion, due to increased loading of the knee joint during the former phase of swinging movement of the leg than the latter.

Figure 5 shows the ROC plots for the FLDA and RBFN classifiers, including the LOO procedure, using the set of features $\{\text{FF1}, \text{FF2}, S, K, H\}$. The A_z value of 0.72 for the FLDA/LOO classifier is comparable to that of FF or FF1 on its own. The highest A_z value obtained was 0.82 using the RBFN classifier with $\sigma = 6$ and $I = 23$ hidden nodes; see Table 2.

The proposed statistical parameters were also computed and evaluated after normalizing each VAG signal to have zero mean and unit standard deviation. No significant differences were observed in the results.

4 Discussion

In preceding works on the analysis of VAG signals, Chu et al. [11–14] reported that specific acoustic patterns related to rheumatoid arthritis, degenerative arthritis, chondromalacia patella, and osteochondritis could be recorded. Kernohan et al. [29–32], Mollan et al. [44], and McCoy et al. [41] demonstrated the importance of the lower frequencies present in VAG signals, which are

Table 2 Performance of the features used for the screening of VAG signals in terms of the area A_z under the ROC curve

Feature	A_z	Standard error
FF	0.72	0.054
FF1	0.73	0.053
FF2	0.68	0.056
S	0.70	0.055
K	0.61	0.059
H	0.60	0.060
FLDA/LOO	0.72	0.054
RBFN/LOO	0.82	0.045

FF, FF1, FF2: Form factor for the full duration, the first half (extension), and the second half (flexion), respectively. S Skewness, K kurtosis, H entropy, *FLDA* Fisher's linear discriminant analysis, *LOO* leave-one-out cross validation, *RBFN* classification using a neural network with radial basis functions. The experiments with FLDA and RBFN were performed using the set of features {FF1, FF2, S , K , H }

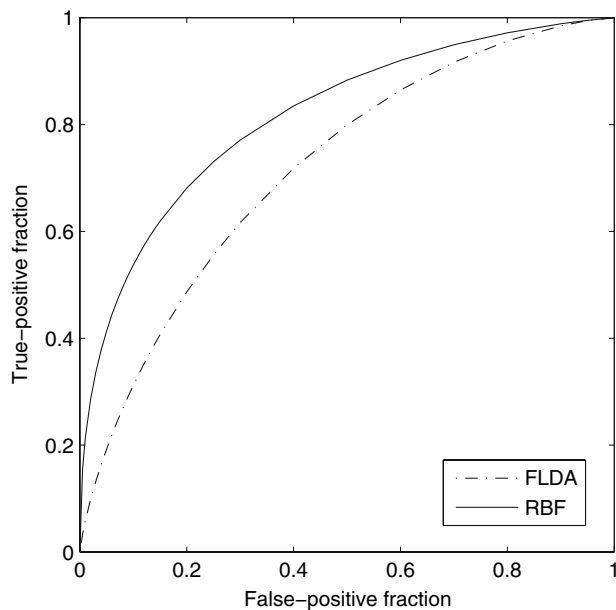


Fig. 5 ROC plots for the FLDA and RBF classifiers, including the LOO procedure, using the set of features {FF1, FF2, S , K , H }. The corresponding areas under the ROC curves (A_z) are 0.72 and 0.82, respectively

missed by acoustic microphones but captured by piezoelectric accelerometers (contact sensors). McCoy et al. [41] found that 80% of the patients with meniscal injuries produced characteristic signals, and that alterations in normal joint crepitus (grinding noise) may be a useful indicator of early cartilage degeneration.

Physiological patello-femoral crepitus (PPC) is a random sequence of vibration pulses apparently generated between the patellar and femoral surfaces, typically

observed during slow knee movement [1–5, 28, 30]. Beverland et al. [2–5] and Kernohan et al. [30] noted that two components—the rate of pulse repetition and the spectrum of the basic signal pulse—affect the spectrum of the PPC signal. Although they described both components and further noted that there are peaks in the PPC spectrum at multiples of the pulse repetition rate, Beverland et al. [2–5] provided no information on whether and how the PPC spectrum could be affected by the inter-pulse interval (IPI) variation which exists in PPC signals. Zhang et al. [64] developed a mathematical model, by using the theory of linear systems and random processes, for the patello-femoral pulse (PFP) train produced by slow knee movement, and showed that the spectral peaks shift toward higher frequencies with increasing repetition rates of the PFP; see also Rangayyan [51]. Measurable parameters such as the mean and variance of the PFP train were found to be independent of the PDF of the IPI, but dependent on parameters related to physiological factors.

Reddy et al. [57] studied the application of their noninvasive accelerometry technique [56] for the characterization of vibration signals related to spondyloarthropathy, with the aim of discriminating this type of pathology from other types of knee-joint disorders. The mean power of the knee acceleration signals in the range of 100–500 Hz was found to be significantly different for spondyloarthropathy patients as compared to signals of patients with rheumatoid arthritis.

Segmentation methods could be used to divide the nonstationary VAG signals into quasi-stationary segments so that modeling techniques such as linear prediction may be used. Segmentation is mandatory when relating signal features to specific angles of the joint (that is, positions at which pathological joint surfaces are in contact). Methods based upon fixed segmentation [19, 37] and adaptive segmentation using linear prediction and adaptive modeling [36, 45, 54, 62] have been proposed for the analysis of VAG signals. Using linear prediction and adaptive segmentation, the first dominant pole and the ratio of the power in the 10–100 Hz band to the total power of the segment were computed by Tavathia et al. [62]; distributions of the features suggested that they could be used to distinguish between normal segments and segments corresponding to articular cartilage breakdown of the patella. Classification using discriminant analysis and logistic regression was performed with model parameters, clinical parameters, and a signal variability parameter by Moussavi et al. [45]; a two-step classification procedure was proposed to classify VAG signals based upon analysis of their segments. Least-squares (autoregressive, all-pole, or linear prediction) modeling methods have been studied, and model parameters along with a few clinical parameters and a signal variability parameter have been used as

discriminant features [36, 45, 54]. With a set of 90 signals, including 51 normal cases and 39 cases with various types of joint-related pathology, the best normal-versus-abnormal classification accuracy achieved was 75.6%; a higher accuracy of 85.9% was achieved in the detection of articular cartilage breakdown of the patella, using a limited set of 51 normals but only 20 cases of chondromalacia of the patella.

Ladly et al. [37] demonstrated clear separation between VAG signals of normal knees and knees with articular cartilage damage in terms of measures related to signal power and median frequency (MDF). When averaged over the total swing cycle, they observed up to 112% difference in mean signal power and up to 173% difference in MDF between normal and pathological VAG signals. In the last 60° of knee extension, the differences increased to up to 471% in mean power and 652% in MDF between normal and pathological signals. The study of Ladly et al. [37] indicated evidence that VAG signals can be separated in terms of their power and MDF in the angle range of [60°, 0°]. (Note that average power is related to the variance if there is no DC present in the signal, as is the case with VAG signals.)

A major drawback of the segmentation-based approach lies in associating the clinical information obtained during arthroscopy with the segments of the corresponding VAG signal. It is difficult to define joint angles accurately during arthroscopy, due to the presence of drapes and surgical equipment. Furthermore, it is difficult to determine the actual points of cartilage contact during load on the joint, because arthroscopy, by design, is performed in an unloaded position with the scope inserted between the joint surfaces. Visualization of a cartilage defect or injury is achieved when it is not in contact with the corresponding articulating surface; when contact is made, the defect is out of view. The angle estimated is a guess by extrapolating, from the arthroscopic visualization, the probable joint angle at which contact between the cartilage surfaces under consideration is maximal. These problems make it difficult to estimate accurately the joint angle related to contact of specific cartilage positions.

Segmentation and joint angle estimation may be avoided by using nonstationary signal analysis tools, such as time-frequency distributions (TFDs) [34, 53]. Using the matching pursuit TFD, Krishnan et al. [34] computed several features to characterize VAG signals. With a set of 90 signals, including 51 normal cases and 39 cases with various types of joint-related pathology, the best normal-versus-abnormal classification accuracy achieved was 68.9%. However, with a reduced set including 51 normals but only 20 cases of chondromalacia of the patella, the accuracy increased to 77.5%. The areas (A_c) under the ROC

curves for the two sets of signals were 0.68 and 0.75, respectively.

Recently, Umopathy and Krishnan [63] applied wavelet packet decomposition and a modified local discriminant bases algorithm to a set of 89 VAG signals. Multiple dissimilarity measures were used to identify an optimal set of discriminant basis functions. The application of a classifier based on linear discriminant analysis led to a normal-versus-abnormal classification accuracy of 79.8%.

Jiang et al. [27] applied vibration arthrometry for the diagnosis of meniscal tear in knee joints, with an overall accuracy of 81% with 37 patients. Jiang et al. [26] extended the application of VAG signal analysis to artificial knee joints. The root-mean-squared (RMS) value and parameters of autoregressive models were used to analyze the signals. The methods could detect and distinguish between failure of the prostheses due to wear of the polyethylene in the patellar component and wear of the metallic components.

In comparison with the results reported in preceding studies on the analysis of VAG signals, the results obtained in the present study are significant in that the statistical parameters derived from the VAG signals, with no segmentation other than splitting the duration of each signal in halves, have provided screening accuracies comparable to those obtained with more sophisticated methods based upon adaptive segmentation, AR modeling [36, 54], cepstral coefficients [54], TFDs [34], and wavelet packet decomposition [63]. The proposed methods do not require any clinical information regarding the patient, reports related to auscultation of the knee joint, or clinical interpretation of the VAG signals. The elimination of the segmentation process obviates the need to estimate the joint angle corresponding to the pathology as observed during clinical examination, auscultation, or arthroscopy. However, the use of the simpler statistical features has required the application of a sophisticated pattern classifier (RBFN) to achieve good classification accuracy. Advanced classifiers such as RBFNs pose concomitant problems related to the derivation of the optimal parameters and generalization from a training set to a test set, among others. Experiments were also conducted with support vector machines (SVMs) for classification of VAG signals using the proposed features; however, the results were not satisfactory.

Further work is in progress on the derivation of additional parameters related to the complexity of the waveforms. We are also conducting further investigations on advanced methods for feature selection, nonlinear pattern classification, and the optimization of the parameters of the classifier [46].

5 Conclusion

The proposed methods have shown good potential for noninvasive screening for articular cartilage pathology, and could lead to a practical approach for the analysis of the nonstationary VAG signals. Our aim is to develop a simple screening tool for use in the clinic of a physician or an orthopedic specialist. Further work is being conducted on the implementation of the proposed techniques on a digital signal processor (DSP) chip that could be located in a stand-alone device or incorporated into a computer. Given the simple nature of the data acquisition and proposed signal analysis procedures, the assessment of the knee joints of a subject could be performed in the office of a physician or in the field in about 10–15 min. Improved selection of patients for further clinical or surgical procedures, such as arthroscopy, could reduce costs to the healthcare system and the associated risks to the patient.

Acknowledgments This work was supported by the Doctoral Program Foundation of the Ministry of Education of China under Grant No. 20060013007 awarded to Y. F. Wu, and by the University of Calgary in the form of a “University Professorship” awarded to R. M. Rangayyan. We thank Dr. Cyril B. Frank and Dr. G. Douglas Bell, Department of Surgery and Sport Medicine Centre, University of Calgary, for their contributions to previous related projects.

References

- Barr DA, Long L, Kernohan WG, Mollan RAB (1994) Continuous passive motion in computer assisted auscultation of the knee. *Comput Meth Prog Biomed* 43:159–169
- Beverland DE, Kernohan WG, Mollan RAB (1985) Analysis of physiological patello-femoral crepitus. In: Byford GH (ed) *Technology in health care*. Biological Engineering Society, London, pp 137–138
- Beverland DE, Kernohan WG, Mollan RAB (1985) Problems in the analysis of vibration emission from the patello-femoral joint. *Med Bio Eng Comput* 23(Suppl 2):1253–1254
- Beverland DE, Kernohan WG, Mollan RAB (1985) What is physiological patello-femoral crepitus? *Med Bio Eng Comput* 23(Suppl 2):1249–1250
- Beverland DE, McCoy GF, Kernohan WG, Mollan RAB (1986) What is patellofemoral crepitus? *J Bone Joint Surg* 68-B:496
- Binnie CD, Batchelor BG, Bowring PA, Darby CE, Herber L, Lloyd DSL, Smith DM, Smith GF, Smith M (1978) Computer-assisted interpretation of clinical EEGs. *Electroencephal Clin Neurophysiol* 44:575–585
- Binnie CD, Batchelor BG, Gainsborough AJ, Lloyd DSL, Smith DM, Smith GF (1979) Visual and computer-assisted assessment of the EEG in epilepsy of late onset. *Electroencephal Clin Neurophysiol* 47:102–107
- Bircher E (1913) Zur diagnose der meniscusluxation und des meniscusabrisses. *Zentralbl f Chir* 40:1852–1857
- Blodgett WE (1902) Auscultation of the knee joint. *Boston Med Surg J* 146(3):63–66
- Chen S, Cowan CFN, Grant PM (1991) Orthogonal least squares learning algorithm for radial basis function networks. *IEEE Trans Neural Net* 2(2):302–309
- Chu ML, Gradisar IA, Mostardi R (1978) A noninvasive electroacoustical evaluation technique of cartilage damage in pathological knee joints. *Med Bio Eng Comput* 16:437–442
- Chu ML, Gradisar IA, Railey MR, Bowling GF (1976) Detection of knee joint diseases using acoustical pattern recognition technique. *J Biomech* 9:111–114
- Chu ML, Gradisar IA, Railey MR, Bowling GF (1976) An electro-acoustical technique for the detection of knee joint noise. *Med Res Eng* 12(1):18–20
- Chu ML, Gradisar IA, Zavodney LD (1978) Possible clinical application of a noninvasive monitoring technique of cartilage damage in pathological knee joints. *J Clin Eng* 3(1):19–27
- Cooper R, Osselton JW, Shaw JC (1980) *EEG technology*, 3rd edn. Butterworths, London
- Duda RO, Hart PE (1973) *Pattern classification and scene analysis*. Wiley, New York
- Erb KH (1933) Über die möglichkeit der registrierung von gelenkgeräuschen. *Deutsche Ztschr f Chir* 241:237–245
- Fischer H, Johnson EW (1960) Analysis of sounds from normal and pathologic knee joints. In: *Proc 3rd intl congr phys med*, pp 50–57
- Frank CB, Rangayyan RM, Bell GD (1990) Analysis of knee sound signals for non-invasive diagnosis of cartilage pathology. *IEEE Eng Med Biol Mag* 9(1):65–68
- Haykin S (2002) *Neural networks: a comprehensive foundation*, 2nd edn. Prentice-Hall PTR, Englewood Cliffs
- Hjorth B (1970) EEG analysis based on time domain properties. *Electroencephal Clin Neurophysiol* 29:306–310
- Hjorth B (1973) The physical significance of time domain descriptors in EEG analysis. *Electroencephal Clin Neurophysiol* 34:321–325
- Hjorth B (1975) Time domain descriptors and their relation to a particular model for generation of EEG activity. In: Dolce G, Künkel H (eds) *CEAN: computerised EEG analysis*, Gustav Fischer, Stuttgart, pp 3–8
- Inoue J, Nagata Y, Suzuki K (1986) Measurement of knee joint sounds by microphone. *Sangyo Ika Daigaku Zasshi* 8(3):307–316
- Jackson RW, Abe I (1972) The role of arthroscopy in the management of disorders of the knee: An analysis of 200 consecutive examinations. *J Bone Joint Surg* 54-B:310–322
- Jiang CC, Lee JH, Yuan TT (2000) Vibration arthrometry in the patients with failed total knee replacement. *IEEE Trans Biomed Eng* 47(2):218–227
- Jiang CC, Liu YJ, Hang YS (1995) Vibration arthrometry for the diagnosis of meniscal tear of the knee. *J Orthop Surg Rep China* 12:1–5
- Jiang CC, Liu YJ, Yip KM, Wu E (1993) Physiological patellofemoral crepitus in knee joint disorders. *Bull Hosp Joint Dis* 53(4):22–26
- Kernohan WG, Barr DA, McCoy GF, Mollan RAB (1991) Vibration arthrometry in assessment of knee disorders: the problem of angular velocity. *J Biomed Eng* 13:35–38
- Kernohan WG, Beverland DE, McCoy GF, Hamilton A, Watson P, Mollan RAB (1990) Vibration arthrometry. *Acta Orthop Scand* 61(1):70–79
- Kernohan WG, Beverland DE, McCoy GF, Shaw SN, Wallace RGH, McCullagh GC, Mollan RAB (1986) The diagnostic potential of vibration arthrography. *Clin Orthop Rel Res* 210:106–112
- Kernohan WG, Mollan RAB (1982) Microcomputer analysis of joint vibration. *J Microcomp Appl* 5:287–296
- Kotani K, Suzuki K (1983) Acoustic analysis of joint-sound through passive motion with special reference to degenerative osteoarthritis of the knee joints. *Nippon Seikeigeta Gakkai Zasshi* 57:1869–1880

34. Krishnan S, Rangayyan RM, Bell GD, Frank CB (2000) Adaptive time-frequency analysis of knee joint vibroarthrographic signals for noninvasive screening of articular cartilage pathology. *IEEE Trans Biomed Eng* 47(6):773–783
35. Krishnan S, Rangayyan RM, Bell GD, Frank CB (2001) Auditory display of knee-joint vibration signals. *J Acoust Soc Am* 110(6):3292–3304
36. Krishnan S, Rangayyan RM, Bell GD, Frank CB, Ladly KO (1997) Adaptive filtering, modelling, and classification of knee joint vibroarthrographic signals for non-invasive diagnosis of articular cartilage pathology. *Med Bio Eng Comput* 35:677–684
37. Ladly KO, Frank CB, Bell GD, Zhang YT, Rangayyan RM (1993) The effect of external loads and cyclic loading on normal patellofemoral joint signals. *Spl Iss Biomed Eng Def Sci J (India)* 43:201–210
38. Lund F, Nilsson BE (1980) Arthroscopy of the patello-femoral joint. *Acta Orthop Scand* 51:297–302
39. Mankin HJ (1982) The response of articular cartilage to mechanical injury. *J Bone Joint Surg* 64-A:462–466
40. Marques de Sá JP (2003) *Applied Statistics using SPSS, STATISTICA, and MATLAB*. Springer, Berlin
41. McCoy GF, McCrea JD, Beverland DE, Kernohan WG, Mollan RAB (1987) Vibration arthrography as a diagnostic aid in diseases of the knee. *J Bone Joint Surg* 69-B(2):288–293
42. Metz CE (1978) Basic principles of ROC analysis. *Sem Nucl Med* VIII(4):283–298
43. Metz CE, Pesce L (2006) *Readings in ROC Analysis, with Emphasis on Medical Applications*; available at www.radiology.uchicago.edu/http://www.edu/krl/KRL_ROC/ROC_analysis_by_topic4.htm. University of Chicago, Chicago
44. Mollan RAB, Kernohan WG, Watters PH (1983) Artefact encountered by the vibration detection system. *J Biomech* 16(3):193–199
45. Moussavi ZMK, Rangayyan RM, Bell GD, Frank CB, Ladly KO, Zhang YT (1996) Screening of vibroarthrographic signals via adaptive segmentation and linear prediction modeling. *IEEE Trans Biomed Eng* 43(1):15–23
46. Mu T, Nandi AK, Rangayyan RM (2007) Strict 2-surface proximal classification of knee-joint vibroarthrographic signals. In: *Proc. 29th ann intl conf IEEE eng med bio soc. IEEE, Lyon*, pp 4911–4914
47. Nagata Y (1988) Joint-sounds in gonarthrosis—clinical application of phonoarthrography for the knees. *J Univ Occup Environ Health Japan* 10(1):47–58
48. Nagata Y, Suzuki K, Kobayashi Y, Sasaki M, Inoue J, Takyu H (1986) Joint-sounds clinical experience of the knee joint. *Sangyo Ika Daigaku Zasshi* 8:425–428
49. Peylan A (1953) Direct auscultation of the joints (preliminary clinical observations). *Rheumatolgy* 9:77–81
50. Rabin EL, Ehrlich MG, Cherrack R, Abermathy P, Paul IL, Rose RM (1978) Effect of repetitive impulsive loading on the knee joints of rabbits. *Clin Orthop* 131:288
51. Rangayyan RM (2002) *Biomedical signal analysis—a case-study approach*. IEEE/Wiley, New York
52. Rangayyan RM (2005) *Biomedical image analysis*. CRC, Boca Raton
53. Rangayyan RM, Krishnan S (2001) Feature identification in the time-frequency plane by using the Hough–Radon transform. *Patt Recog* 34:1147–1158
54. Rangayyan RM, Krishnan S, Bell GD, Frank CB, Ladly KO (1997) Parametric representation and screening of knee joint vibroarthrographic signals. *IEEE Trans Biomed Eng* 44(11):1068–1074
55. Rangayyan RM, Wu YF (2007) Analysis of knee-joint vibroarthrographic signals using statistical measures. In: *Proc. 20th IEEE intl symp computer-based med sys. IEEE, Maribor*, pp 377–382
56. Reddy NP, Rothschild BM, Mandal M, Gupta V, Suryanarayanan S (1995) Noninvasive acceleration measurements to characterize knee arthritis and chondromalacia. *Ann Biomed Eng* 23:78–84
57. Reddy NP, Rothschild BM, Verrall E, Joshi A (2001) Noninvasive measurement of acceleration at the knee joint in patients with rheumatoid arthritis and spondyloarthropathy of the knee. *Ann Biomed Eng* 29(12):1106–1111
58. Sasaki M, Suzuki K, Inoue J (1991) Analysis and application of joint sounds to osteoarthritis of the knee. *Trans Comb Meet Orthop Res Soc, USA, Japan and Canada*, p 164
59. Shen YP, Rangayyan RM, Bell GD, Frank CB, Zhang YT, Ladly KO (1995) Localization of knee joint cartilage pathology by multichannel vibroarthrography. *Med Eng Phys* 17(8):583–594
60. Steindler A (1937) Auscultation of joints. *J Bone Joint Surg* 19(1):121–136
61. Szabo E, Danis L, Torok Z (1972) Examination of the acoustic phenomena observed in the knee. *Traumatologia* 15(2):118–127
62. Tavathia S, Rangayyan RM, Frank CB, Bell GD, Ladly KO, Zhang YT (1992) Analysis of knee vibration signals using linear prediction. *IEEE Trans Biomed Eng* 39(9):959–970
63. Umapathy K, Krishnan S (2006) Modified local discriminant bases algorithm and its application in analysis of human knee joint vibration signals. *IEEE Trans Biomed Eng* 53(3):517–523
64. Zhang YT, Frank CB, Rangayyan RM, Bell GD (1992) Mathematical modeling and spectrum analysis of the physiological patello-femoral pulse train produced by slow knee movement. *IEEE Trans Biomed Eng* 39(9):971–979
65. Zhang YT, Rangayyan RM, Frank CB, Bell GD (1994) Adaptive cancellation of muscle contraction interference from knee joint vibration signals. *IEEE Trans Biomed Eng* 41(2):181–191